



HAL
open science

Modelling of NO photocatalytic degradation in an experimental chamber

Julie Hot, Erick Ringot, Lounes Koufi, Alexandra Bertron

► **To cite this version:**

Julie Hot, Erick Ringot, Lounes Koufi, Alexandra Bertron. Modelling of NO photocatalytic degradation in an experimental chamber. Chemical Engineering Journal, 2020, pp.127298. 10.1016/j.cej.2020.127298 . hal-03011175

HAL Id: hal-03011175

<https://hal.science/hal-03011175>

Submitted on 3 Feb 2023

HAL is a multi-disciplinary open access archive for the deposit and dissemination of scientific research documents, whether they are published or not. The documents may come from teaching and research institutions in France or abroad, or from public or private research centers.

L'archive ouverte pluridisciplinaire **HAL**, est destinée au dépôt et à la diffusion de documents scientifiques de niveau recherche, publiés ou non, émanant des établissements d'enseignement et de recherche français ou étrangers, des laboratoires publics ou privés.



Distributed under a Creative Commons Attribution - NonCommercial 4.0 International License

Modelling of NO photocatalytic degradation in an experimental chamber

Julie Hot^{1*}, Erick Ringot², Lounes Koufi¹, Alexandra Bertron¹

¹LMDC, INSA/UPS Génie Civil, 135 Avenue de Rangueil, 31077 Toulouse Cedex 4 France

²LRVision SARL, 13 Rue du Développement, 31320 Castanet-Tolosan France

* Corresponding email: hot@insa-toulouse.fr

Abstract

"Almost real-life" experiments of abatement of a pollutant, actually nitrogen monoxide, were carried out in a 10-m³ chamber, the walls of which were covered with plasterboard samples, themselves coated with a photocatalytic dispersion. The experimental protocol consisted in first injecting NO polluted air into the chamber to a certain level, then maintaining a steady level of pollution by tuning the flow rate to balance the leaks and, finally, illuminating the chamber. In a first stage of analysis, a three-flow (injection, leakage and renewal flows) model was used in order to characterize the leakage flow rate. This model was based on the difference of NO concentration between the interior and the exterior rather than on a pressure difference. A two-parameter empirical law was specially formulated for this purpose. In a second stage, the photocatalytic phenomenon was described by a four-flow model completing the previous one, the fourth flow being associated with the photocatalytic oxidation of NO. This flow was described by a rate law derived from the Langmuir-Hinshelwood (L-H) law, which was generalized to the experimental chamber. The parameters K (adsorption constant) and k (abatement kinetics constant) of the rate law were identified using a standardized lab-scale reactor. The equations, integrated by finite differences, fitted the experimental results correctly. The "diffusive zone thickness" was introduced as the thickness of the air layer potentially concerned by the photocatalysis and was quantified. This first attempt to model photocatalysis on a large scale was promising. However, further research work is needed to enable the model to take more parameters into account.

Keywords

Langmuir-Hinshelwood; Modelling; Photocatalysis; Nitrogen monoxide; Experimental chamber

1. Introduction

Indoor air is polluted by gaseous compounds, which mainly come from building materials, occupant activities and outdoor pollution. As an example, nitrogen oxides, which are harmful outdoor pollutants emitted by transport vehicles and industries, often infiltrate buildings. Two main strategies may be adopted to decrease indoor pollutant concentration: (1) source control, which consists in eliminating individual sources of emissions to reduce the global pollution, and/or (2) remediation action, which involves combatting the existing pollution with techniques such as mechanical ventilation, air cleaning devices or air-depollution coating. However, an improved ventilation system may bring in a higher volume of outdoor air, which can be problematic in the vicinity of heavy traffic areas where levels of traffic-related pollutants are high. Several air purifiers and air-depollution coatings work by using photocatalysis. This well-known technique is based on the photo-activation of a metal-oxide semiconductor. Under irradiation (with photons of higher energy than that of the bandgap), electron-hole pairs are created, leading to the formation of reactive radicals (such as hydroxyl OH^{\bullet} and superoxide $\text{O}_2^{\bullet-}$), which allow the mineralization of gaseous pollutants through redox reactions. This use of heterogeneous photocatalysis to reduce the concentration of nitrogen oxides ($\text{NO}_x = \text{NO} + \text{NO}_2$) has been largely reported in the literature. Nitrogen monoxide (NO) has been used as a probe molecule in numerous studies, mainly because it does not adsorb on/react with the surfaces to any notable extent and can be easily measured by a chemiluminescent analyzer [1]. The successive reactions of its photo-oxidation lead to nitrate species end-products via the formation of NO_2 (nitrogen dioxide) [2,3]. The efficiency of the photocatalytic process has been largely evaluated at a lab scale using standardized methods and reactors [2,4,5]. In such conditions, the influence of environmental parameters, such as humidity, temperature, concentration, illumination intensity, substrate type, and of the semiconductor physicochemical properties have been investigated, as they can be controlled [6–10]. Several research works have also been carried out at larger scales (tunnel, road pavement, canyons, etc.) under environmental conditions and ambient pollution [11,12]. The reported observations highlight the variability of the removal rate results because of their dependence on numerous parameters, such as light intensity and energy, wind speed and ambient pollution, which makes it difficult to predict the process efficiency in real conditions. From a modelling point of view, the Langmuir-Hinshelwood (L-H) model has been widely used in the literature to describe the photocatalytic reaction rate of NO and other chemical pollutants at a reactor scale [13–16]. Modelling provides a reasonable interpretation of the experimental data and is an interesting tool to predict the decrease of a gaseous pollutant concentration under various conditions [17]. This was notably highlighted by Hunger et al., who derived a model of the NO decomposition process occurring on a photocatalytic concrete paving

stone in a reactor cell in order to predict its performance under various conditions and thus to envisage the translation of this process to real-scale applications [18].

This paper reports the first step of research work aimed at modelling the photocatalytic reaction in an experimental chamber. The objectives were twofold: (1) to understand the diminution of gaseous pollutant concentration in indoor conditions and, in particular, to identify the contribution of air leakage, air renewal and photocatalytic oxidation (as a technique of air pollution remediation), and (2) to predict the efficiency of photocatalytic devices/products for improving indoor air quality. The gaseous pollutant and semiconductor tested were nitric oxide, NO, and titanium dioxide, TiO₂, respectively. A rate law similar to the L-H model was used at reactor scale to identify the kinetic constant and the NO adsorption coefficient under UV-A and visible light. Then, a model was built at the chamber scale, based on three or four flows depending on whether or not the photocatalysis was active. The NO pollution flows corresponded to the artificial injection, the outdoor pollution, the leakage, and the photocatalytic degradation.

2. Materials and experimental procedures

2.1. Materials

Experiments in the lab reactor were carried out with two common building materials as substrates: painted plasterboard and mortar. The samples placed inside the reactor were rectangular: 100 mm or 250 mm long, 50 mm wide and 10 mm thick. Commercial plasterboard (Placoplatre® BA 13) was cut into samples of the desired dimensions and then painted with orange water-based acrylic paint (LRVision). The formulation and preparation of the mortar were adapted from the NF EN 196-1 standard [19]. Siliceous sand and CEM I 52.5 Portland cement were used. They were mixed mechanically with water (at a water to cement ratio (W/C) of 0.5) at ambient temperature and humidity for 3.5 min and then cast in a 300 × 300 × 10 mm³ steel mold with the aid of a vibrating table. The slab was demolded after 5 days and sawn into samples of the desired dimensions. Finally, the mortar surfaces were ground (120-mm abrasive sandpaper).

Tests in the experimental chamber were conducted with plasterboard samples only. Commercial plasterboards (Placoplatre® BA 13) were cut into pieces of specific dimensions to fit the indoor walls of the experimental chamber (100 × 50 cm², 75 × 50 cm², 50 × 50 cm² and 50 × 25 cm²) and covered an indoor surface of 9.8 m². The edges of each plate were protected with adhesive tape and the surfaces were painted as for samples in the reactor.

The TiO₂ particles were stabilized in an aqueous suspension to ensure the safety of the operator during the application (no risk of inhalation). The photocatalytic dispersion was applied with a brush at the surface of each substrate. It was prepared from a formulated water-based commercial product

(CristalACTiV™ S5-300B, ultrafine TiO₂ anatase particles at 18 wt%) by dilution with demineralized water. The TiO₂ particles had a diameter of around 50 nm and the TiO₂ dry content at the surface after application was 5 g/m² for all the samples (used in the reactor and in the experimental chamber). This value was chosen in order to obtain a high photocatalytic depollution efficiency and thus make it possible to carry out the modelling work.

2.2. Experiments at reactor scale

2.2.1. Description of the setup

The experimental setup used to assess the photocatalytic degradation of NO at a lab scale is described in more detail in [10]. It consisted of three parts: (1) a polluted air supply mixing NO (8 ppm of NO stabilized in N₂, Air Liquide™) with humidified and dry air streams adjusted by mass flow controllers MFC (Bronkhorst); (2) the lighting system and the photocatalytic reactor (cylindrical shape, free volume = 424 cm³) containing a sample, which was swept by the polluted air; (3) a NO_x chemiluminescent analyzer (ENVEA Environnement SA, France, model AC32M), which measured the concentration of NO_x, NO and NO₂ ($[NO_2] = [NO_x] - [NO]$) at the exit of the reactor. In order to control and adjust the NO initial concentration, the polluted air was also sent through a bypass directly to the analyzer. The temperature and the relative humidity were kept constant at 21 ± 2 °C and 50 ± 5 % respectively.

2.2.2. Experimental protocol

The experimental protocol took its inspiration from standard ISO 22197-1 [20]. The NO flow rate was set at 1.50 l/min. Initial NO concentrations varied between 50 and 400 ppb. Two lighting conditions were tested: visible light (fluorescent tube, Osram T8 Lumilux Cool White L 18W 840) and UV-A light (fluorescent tube, Narva LT-T8 Blacklight blue 30W 073). The lighting intensity received by the sample surface was measured by a radiometer (Gigahertz-Optik) using two detectors (UV-A, UV-3717 model and visible, RW-3703 model). The values obtained were 6 W/m² for visible wavelengths (400-800 nm) and 1 W/m² for UV-A wavelengths (315-400 nm). The light spectrum of the visible fluorescent tube is shown in [21]. The main steps of the protocol were: (1) injection of NO polluted air through the bypass to check the initial level – light off (5 min), (2) injection of NO polluted air through the reactor containing a sample - light off (15 min), (3) switching on of the light to activate the photocatalysis (60 min), (4) switching off of the light to stop the photocatalysis (15 min), and (5) calculation of the NO photocatalytic efficiency ξ (in %) (cf. part 3.1). The steps of this protocol are schematically represented in [10,22]. The experiments carried out in the reactor allowed the two constants of the assumed L-H kinetics to be identified, as explained in part 3.1. Each experiment (same initial concentration and lighting condition) was conducted three times with a different mortar sample each time.

2.3. Experiments at chamber scale

2.3.1. Description of the setup

The macro-scale experiments were carried out in an experimental house located at the LMDC (France). This setup was previously described in [21,23]. It was divided into two rooms of 10 m³ each. One room – the experimental chamber – was used as a photocatalytic reactor and contained the samples (covering a wall surface area of 9.8 m²), and ventilation and lighting systems. The second room – the monitoring chamber – was equipped with a NO_x analyzer (HORIBA APNA370) and a gas cylinder (45 ppm of NO stabilized in N₂, Air Liquide) connected to an MFC (M+W Instruments™ Mass-Stream). A fan was necessary to homogenize the atmosphere. The two rooms were connected with stainless steel tubes: one enabling the NO_x analyzer to sample gas for measurement, the other for injecting the pollutant from a gas cylinder through the MFC. Meteorological data (environmental parameters) were acquired using a weather station (DAVIS Vantage Pro2™). Humidity and temperature inside the photocatalytic room were also acquired using a data logger (KIMO KH60). The values were 50 ± 10 % and 20 ± 5 °C, respectively. Moreover, indoor/outdoor exchanges occurred due to 'natural' leakage because, among other reasons, the joinery was not perfectly airtight.

2.3.2. Experimental protocol

NO artificial pollution was injected into the experimental chamber as described in [21]. Two protocols were followed to identify the model parameters as explained in part 3.2. Each protocol consisted of 4 main steps; the first three, conducted in the dark, were identical for both protocols, the last one was different as described below:

- (1) background NO_x level assessment;
- (2) fast NO dynamic injection at 1.5 l/min until the desired concentration was reached inside the chamber;
- (3) NO injection at a lower flow rate to compensate for air leakage and maintain the pollution at the desired concentration (concentration plateau), and
 - (4.a) stopping of the injection (cf. part 3.2, modelling without the photocatalytic activity), or
 - (4.b) keeping the low injection rate and switching on the light to activate the photocatalysis (cf. part 3.2, modelling with the photocatalytic activity under artificial light). The photocatalysis was activated with visible light (4 fluorescent tubes, Sylvania T8 Luxline Plus 30W 840) or UV-A light (4 fluorescent tubes, Narva LT-T8 Blacklight blue 30W 073).

Experiments with three different maximum concentrations, expressed in ppb, were carried out. Their values and the corresponding injection flow rates used to maintain a constant pollution level are summarized in Table 1. Experiments without the photocatalytic activity were carried out three times for each concentration (cf. part 4.2.1). Only one experiment was conducted with the photocatalytic activity for each lighting condition, UV-A and visible light (cf. part 4.2.2).

Table 1. Maximum concentrations injected in the experimental chamber and the corresponding injection flow rates to maintain the concentration at a stable level.

Maximum concentration reached in the experimental chamber (ppb)	Injection flow rate to maintain the concentration constant in the chamber (ln/min)
300	0.45
200	0.30
100	0.20

2.4. Differences between the reactor and the chamber

In the lab-scale reactor, the gas flow is pushed from one edge to the other by a piston effect. The pollutant concentration decreases progressively during its journey along the photocatalyst applied to the sample surface. The thickness of the air layer is 5 mm according to standard ISO 22197-1 [20]. Therefore, all the pollutant flow is assumed to be concerned by the abatement.

The experimental chamber is not standardized. Its interest is that it simulates a room close to a real one (even if the size of 10 m³ remains modest in regard to the volume of real rooms). The pollutant invades all the volume so a significant part of the polluted gas, far from the walls, is little concerned by the abatement, if at all.

The lab-scale enables the set {surface + photocatalyst + illuminant} to be characterized via coefficients k and K of the L-H-like model. In turn, these factors are used in the four-flow model, provided the walls were coated by the same materials and lit by the same light.

The reactor is airtight; the chamber presents a slight air infiltration/exfiltration, which is not controlled but is taken into account in the modelling (cf. part 3.2).

3. Model description

The following sections discuss the model development.

3.1. Langmuir-Hinshelwood-like model in the reactor

The Langmuir-Hinshelwood (L-H) approach has been widely used to analyze the kinetics of heterogeneous photocatalysis at a lab scale. The photocatalytic reaction is closely related to the L-H adsorption model as its rate depends on the coverage of the semiconductor particle surface by the

gaseous pollutant. Peral and Ollis notably employed this model to describe the photocatalytic oxidation of 1-butanol, formaldehyde, and m-xylene when the surface of a porous fritted glass plate covered with a P25 TiO₂ powder layer (anatase) was irradiated under UV [24]. Sleiman et al. investigated the photocatalytic removal of toluene at indoor air levels using an annular flow-through reactor with TiO₂ as photocatalyst [25]. They showed that the experimental data complied with the L-H rate expression. Such a model was also applied to describe NO_x photocatalytic oxidation. Devahasdin et al. showed that the steady-state experimental data obtained for space time and inlet concentration effect studies were well fitted by the L-H kinetic model, which took the reaction rate constants of the catalyst TiO₂ and the adsorption equilibrium constants of NO, NO₂ and H₂O into account [26]. Moreover, Ballari et al. proposed an extended kinetic model based on L-H, which included the relative humidity and irradiance effects. They showed good agreement between the model predictions and experimental results for NO and NO₂ concentrations [27].

In the reactor presented previously, the air flow is “pushed” along the photocatalytic surface of a sample (mortar or plaster), and becomes less and less polluted, provided the irradiation is sufficient to activate the semiconductor particles. A rate law, inspired from the L-H model, whose expression is given by equation (1), was used to describe the kinetics of the NO consumption in the reactor due to the photocatalysis process. The negative sign of this expression is consistent with the abatement of NO due to photocatalysis.

$$\dot{\eta} = \frac{d\eta}{dt} = -\frac{kK\eta}{1+K\eta} = -\frac{k}{1+\frac{1}{K\eta}} \quad (\text{eq.1})$$

In this equation, $\dot{\eta}$ represents the disappearance rate of the reactant (the variation of the NO pollutant concentration per increment of time) expressed in ppb/min and η is the reactant concentration in ppb (η_0 being the concentration at the entrance of the reactor). As for the L-H law, this model involves two specific coefficients: K , expressed in ppb⁻¹, which is the adsorption equilibrium constant and defines the gas/surface adsorption affinity, and k , expressed in ppb/min, which is the reaction rate constant. The latter parameter has to be considered as a pseudo-first order factor describing the kinetics of NO abatement, involving the intermediate reactions of oxygen, vapour, hydroxyl radical formation and combination with NO.

Figure 1 gives a schematic representation of the polluted air flowing on the surface of a sample in the reactor. The sample is characterized by its length, L , and width, b . The air layer above the sample, i.e. in the space between the sample surface and the upper surface of the reactor, has a thickness $e = 5 \text{ mm}$. At steady state and $x + dx$ abscissa, the concentration inside the reactor is equal to

$\eta(x + dx)$; η_0 and η_1 being the concentrations at the entrance and at the exit of the reactor, respectively.

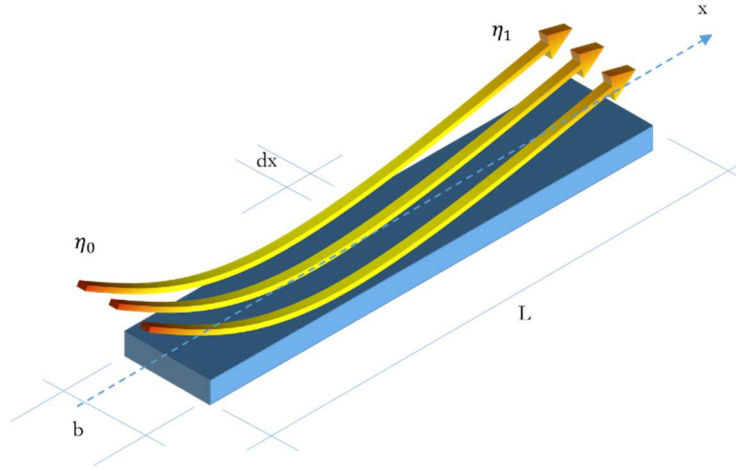


Figure 1. Schematic representation of the polluted air flow on the surface of a sample along the x-axis. L : length, b : width, η_0 : concentration at the entrance and η_1 : concentration at the exit.

In the reactor, the volume of air (v) is injected at a constant flow rate (q) at a speed (u). The flow rate is defined by equation 2 and the speed by equation 3:

$$q = \frac{dv}{dt} \quad (\text{eq.2})$$

$$u = \frac{dx}{dt} = \frac{q}{be} \quad (\text{eq.3})$$

From equations 1 and 3, the variation of the concentration in the reactor ($d\eta$) can be given as a function of the sample length (dx) (equation 4):

$$d\eta = -\frac{kK\eta}{1+K\eta} dt = -\frac{kK\eta}{1+K\eta} \frac{be}{q} dx \quad (\text{eq.4})$$

Equation 4 can be integrated with respect to the limits: $\eta = \eta_0$ at $x = 0$ and $\eta = \eta(x)$ at $x = x$, thus reducing the rate expression to equation 5:

$$\eta(x) - \eta_0 + \frac{1}{K} \ln \frac{\eta(x)}{\eta_0} = -\frac{kbe}{q} x \quad (\text{eq.5})$$

which leads to equation 6 at the exit of the photocatalytic reactor: $\eta = \eta_1$ for $x = L$:

$$\eta_1 - \eta_0 + \frac{1}{K} \ln \frac{\eta_1}{\eta_0} = -\frac{kbe}{q} L \quad (\text{eq.6})$$

The photocatalytic efficiency (ξ) is defined by equation 7 as the relative difference between the NO concentration at the entrance of the reactor, η_0 , and the NO concentration at the exit of the reactor, η_1 :

$$\xi = \frac{\eta_0 - \eta_1}{\eta_0} \quad (\text{eq.7})$$

Therefore, equation 6 can be rewritten as:

$$\xi \eta_0 - \frac{1}{K} \ln(1 - \xi) = \frac{kV_a}{q} \quad (\text{eq.8})$$

where $V_a = beL$ is the volume of the air layer above the upper surface of the sample in the reactor.

Equation 8 implicitly expresses the photocatalytic efficiency as a function of the concentration of polluted air at the entrance of the reactor. This equation can be rewritten as a linear function (equation 9):

$$-\frac{\ln(1-\xi)}{\eta_0 \xi} = \frac{kKV_a}{q} \frac{1}{\eta_0 \xi} - K \quad (\text{eq.9})$$

which can be simply expressed as:

$$Y = AX + B \quad (\text{eq.10})$$

where X and Y are two intermediate variables, defined as follows:

$$\begin{cases} X = \frac{1}{\eta_0 \xi} \\ Y = -\frac{\ln(1-\xi)}{\eta_0 \xi} = -\frac{\ln \eta_0 - \ln \eta_1}{\eta_0 - \eta_1} \end{cases} \quad (\text{eq.11})$$

Like X, Y is positive as $\xi \in [0; 1]$;

A and B are two constants, the slope and the intercept of the straight line respectively, defined by:

$$\begin{cases} A = \frac{kKV_a}{q} \\ B = -K \end{cases} \quad (\text{eq.12})$$

It should be noted that the L-H model is a local adsorption-reaction law, which means that, at reactor scale, a number of influencing parameters are assumed to be uniform as the sample is small. This notably concerns the nature of the substrate, the light intensity, the photocatalytic dispersion applied to the sample surface, the relative humidity and temperature in the vicinity of the photocatalytic surface, and the residence time of the gaseous pollutant in the reactor.

3.2. Three- and four-flow model in the experimental chamber

The model describing the evolution of NO concentration in the experimental chamber was developed in two steps:

- Step 1: modelling without the photocatalytic activity,
- Step 2: modelling with the photocatalytic activity under artificial light (visible or UV-A).

Step 1 allows the air leakage kinetics to be characterized. As reported previously by the authors [23], in the case of a static injection (i.e. the quantity of pollutant injected was controlled by setting the flow rate and the injection volume), the NO concentration naturally decreased when the injection was stopped. This diminution was attributed to the air leakage of the experimental chamber because of imperfect airtightness of the joineries, which allowed part of the polluted air to be exhausted to the outside. Because no differential pressure was detected during experiments, the suggested model is based on the NO concentration difference between indoors and outdoors, which drives the air leakage. As shown in Figure 2.a, three flows are considered, each of them being associated with an NO concentration:

1. q_{inj} is the flow rate of NO injected into the experimental chamber at the concentration η_{inj} ; η_{inj} being the NO concentration in the gas cylinder, i.e. 45 ppm;
2. q_{leak} is the flow rate of the air leakage and η is the indoor NO concentration;
3. q_{ren} is the flow rate of the air renewal and $\bar{\eta}$ the outdoor NO concentration.

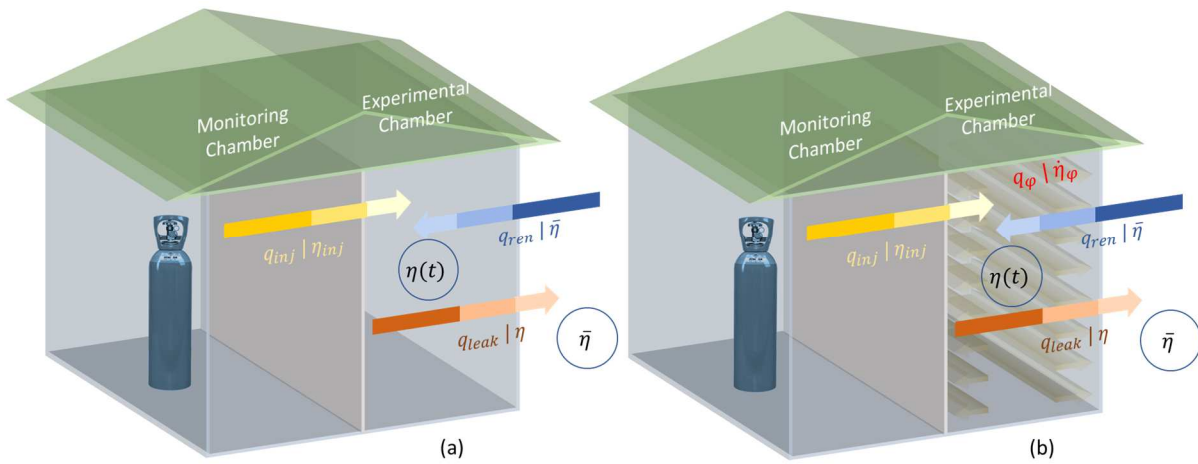


Figure 2. Schematic representation of: a) the three-flow model (step 1), and b) the four-flow model (step 2) in the experimental chamber.

The conservation law for flow rate leads to equation 13:

$$q_{inj} + q_{ren} - q_{leak} = 0 \quad (\text{eq.13})$$

Equation 14 describes the variation of NO concentration ($d\eta$) as a function of time in an experimental chamber of volume V :

$$q_{inj}\eta_{inj}dt + q_{ren}\bar{\eta}dt - q_{leak}\eta dt = d\eta V \quad (\text{eq.14})$$

The air leakage is triggered by the difference between the indoor NO concentration (η) and the outdoor NO concentration ($\bar{\eta}$). The relationship between the leak rate q_{leak} and the difference of NO concentration is expressed via an empirical law introduced by equation 15:

$$q_{leak} = \bar{q} \left[\left(\frac{\eta}{\bar{\eta}} \right) - 1 \right]^\alpha, \eta > \bar{\eta} \quad (\text{eq.15})$$

where \bar{q} is a flow rate-like constant, α is a positive dimensionless number and $\eta > \bar{\eta}$ since the pollutant was artificially injected into the experimental chamber. These two constants are assumed to characterize the behavior of the room. Obviously, q_{leak} vanishes as $\eta \rightarrow \bar{\eta}$. This empirical law also works when $\bar{\eta} > \eta$, provided that it is rewritten:

$$q_{leak} = \text{sign}(\eta - \bar{\eta}) \times \bar{q} \left| \left(\frac{\eta}{\bar{\eta}} \right) - 1 \right|^\alpha \quad (\text{eq.15}')$$

In this way, equation 15' also allows for the possibility that the NO outdoor concentration becomes higher than the NO indoor concentration; in such a case, the flow rate is reversed.

The following differential equation (equation 16) is then obtained from equations 13, 14 and 15:

$$\frac{d\eta}{dt} = \frac{\bar{\eta}}{V} \left[q_{inj} \left(\frac{\eta_{inj}}{\bar{\eta}} - 1 \right) - \bar{q} \left(\frac{\eta}{\bar{\eta}} - 1 \right)^{1+\alpha} \right] \quad (\text{eq.16})$$

Equation 16 expresses the variation of the NO indoor concentration in the experimental chamber as a function of time. The solution of this non-linear differential equation is $\eta(t) = f_{\bar{q},\alpha}(t)$. However, it has no analytical expression. Therefore, it was solved by the finite difference method by running incremental calculations according to the scheme shown in Figure 3. The volume of the experimental chamber (V), the injected flow rate (q_{inj}), the concentration of injected NO (η_{inj}) and the NO outdoor concentration ($\bar{\eta}$) are experimental parameters, which were obtained by measurement. Δt is the timestep and was equal to 5 min here (time interval between two measurements displayed by the analyzer).

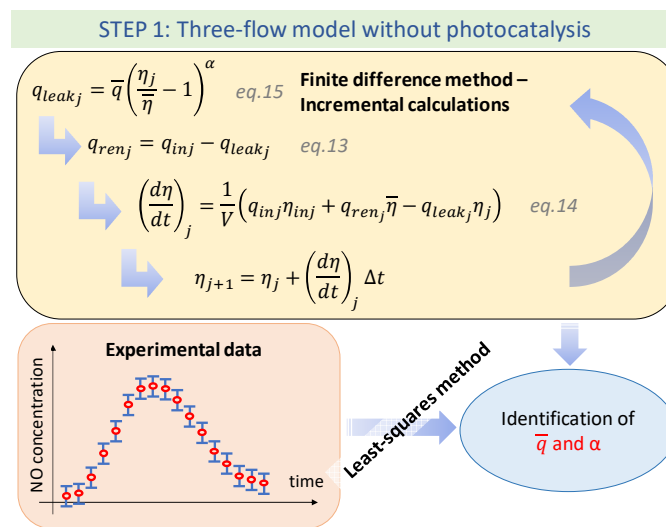


Figure 3. Scheme showing the method implemented to solve equation 16 and identify parameters \bar{q} and α (step 1).

Parameters \bar{q} and α were obtained by the least-squares method (a spreadsheet solver was used). Their optimal values were found by minimizing equation 17, i.e. the sum (χ_2) of squared differences between the measured experimental concentrations (η_j) and the concentrations predicted by the model ($f_{\bar{q},\alpha}(t_j)$).

$$\chi_2 = \sum [\eta_j - f_{\bar{q},\alpha}(t_j)]^2 \quad (\text{eq.17})$$

Step 2 consists in adding a new flow to the model to take the photocatalytic oxidation of NO into account. This additional flow, noted q_φ , is shown in Figure 2.b and is defined according to equation 18:

$$q_\varphi = S \times e' \times \dot{\eta}_\varphi = V_\varphi \times \dot{\eta}_\varphi \quad (\text{eq.18})$$

where S is the surface fonctionnalized by the photocatalytic dispersion, e' is the thickness of the air layer along the sample surface concerned by diffusive, adsorption or degradation phenomena, V_φ is the volume of the polluted air concerned by the photocatalysis and $\dot{\eta}_\varphi$ is the disappearance rate of the NO due to photocatalysis. The thickness of the air layer, which is associated with the free space above the sample surface in the reactor, is unknown in the experimental chamber. This air layer corresponds to the diffusive zone of the reactive radicals (created by the irradiation of the semiconductor particles), which can react with NO molecules, as shown in Figure 4. The rate law inspired from the L-H model, defined by equation 1, was used to express $\dot{\eta}_\varphi$. The assumptions made at the reactor scale (cf. part 3.1) were assumed to be valid for a larger volume. Moreover, equation 1 was simplified to equation 19 as the NO concentrations were around 100 ppb and constant K was of the order of 10^{-4} ppb^{-1} ($1 \gg \frac{1}{100}$).

$$\dot{\eta}_\varphi = \frac{d\eta_\varphi}{dt} = -\frac{Kk\eta}{1+K\eta} \approx -Kk\eta \quad (\text{eq.19})$$

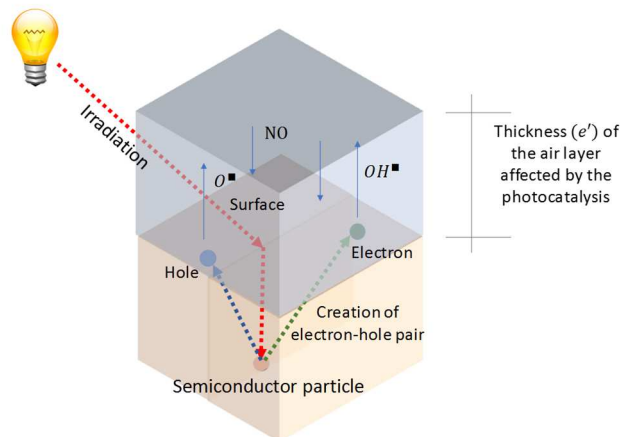


Figure 4. Schematic representation of the thickness e' of the air layer affected by the photocatalysis above the sample surface in the experimental chamber.

Equations 13 and 15 defined in step 1 are kept. However, equation 14 changes to equation 20 to take the variation of the NO concentration due to the photocatalysis into account (the new flow q_φ is added).

$$q_{inj}\eta_{inj}dt + q_{ren}\bar{\eta}dt - q_{leak}\eta dt + V_\varphi d\eta_\varphi = d\eta V \quad (\text{eq.20})$$

The combination of equations 13, 15, 19 and 20 leads to the following differential equation, the solution of which is $\eta(t)$.

$$\frac{d\eta}{dt} = \frac{\bar{\eta}}{V} \left[q_{inj} \left(\frac{\eta_{inj}}{\bar{\eta}} - 1 \right) - \bar{q} \left(\frac{\eta}{\bar{\eta}} - 1 \right)^{1+\alpha} \right] - \frac{V_\varphi}{V} Kk\eta \quad (\text{eq.21})$$

which can be simplified to:

$$\frac{d\eta}{dt} = \frac{\bar{\eta}}{V} \left[q_{inj} \left(\frac{\eta_{inj}}{\bar{\eta}} - 1 \right) - \bar{q} \left(\frac{\eta}{\bar{\eta}} - 1 \right)^{1+\alpha} \right] - A_\varphi \eta \quad (\text{eq.22})$$

where $A_\varphi = \frac{V_\varphi}{V} Kk$ is expressed in min^{-1} .

Parameters \bar{q} and α were defined in step 1 (experiments without photocatalysis) and their values were kept for step 2. The only unknown variable for step 2 was A_φ . The non-linear equation 22 was solved by the finite difference method by running incremental calculations according to the scheme shown in Figure 5.

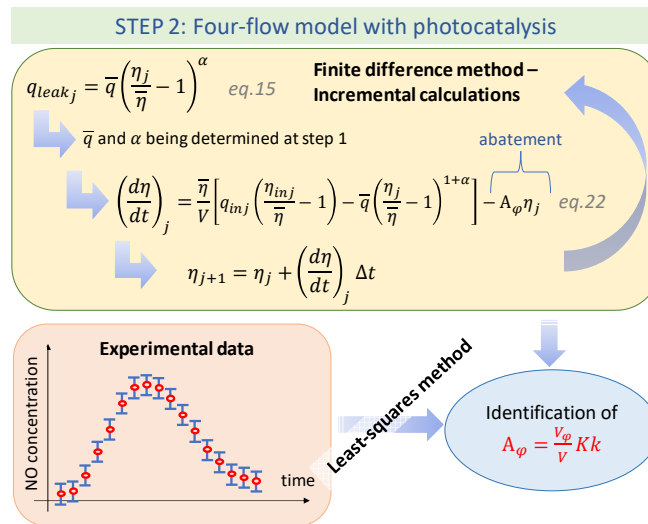


Figure 5. Scheme showing the method implemented to solve equation 22 and identify the parameter A_φ (step 2).

4. Results and discussion

4.1. Determination of the constants at reactor scale

Figure 6 shows the photocatalytic efficiency ξ as a function of the NO concentration η_0 injected into the reactor for mortar samples with the shorter length (100 mm) under visible and UV light. Various

concentrations η_0 were tested: 50, 100, 200, 300 and 400 ppb. The NO concentration η_1 at the exit of the reactor was measured by the analyzer and the photocatalytic efficiency ξ was calculated using equation 7. In Figure 7, the variable $Y = -\frac{\ln \eta_0 - \ln \eta_1}{\eta_0 - \eta_1}$ is plotted as a function of the variable $X = \frac{1}{\eta_0 \xi}$ (cf. equations 9 and 11). A linear relation is clearly observed for both UV-A and visible light, meaning that the L-H-like law was valid. The expressions of the trend lines are reported on Figure 7. Their equations allowed the adsorption coefficients K to be identified ($Y = -K$ for $X = 0$) and the values of k (reaction rate constant) to be determined from the slopes (cf. equations 10 and 12). However, the values obtained for the adsorption coefficient K were negative under both lighting conditions. These results are unexpected and can be explained by the lack of precision of the experimental points – the lines go through the vicinity of the coordinate system origin, near the 0 value, probably because of the low NO adsorption capacity of the exposed surfaces. The uncertainty on the coefficient K therefore becomes higher than the value of the coefficient itself. To overcome this problem, the authors decided to increase the length of the sample in order to obtain higher abatement values. A new series of experiments was conducted with longer samples (250 mm in length instead of 100 mm) and thus with a higher quantity of TiO_2 particles at the surface (the TiO_2 dry content per m^2 was kept constant).

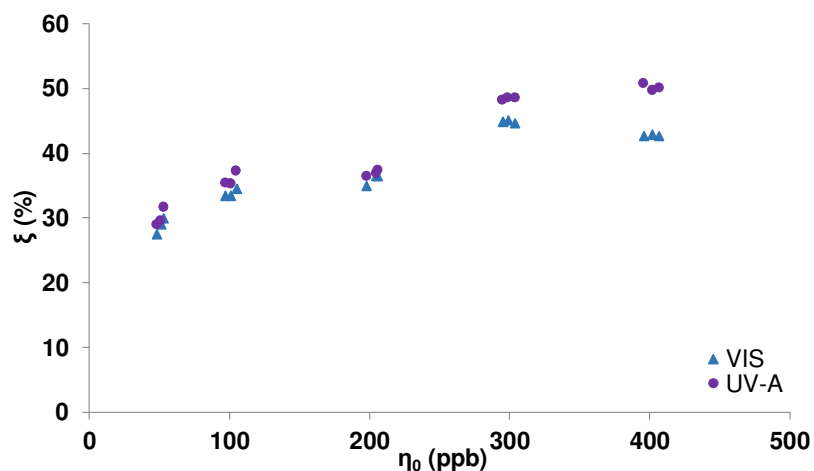


Figure 6. Photocatalytic efficiency ξ (cf. equation 7) as a function of the NO concentration η_0 injected into the reactor for 100 mm long mortar samples under UV-A and visible light (VIS).

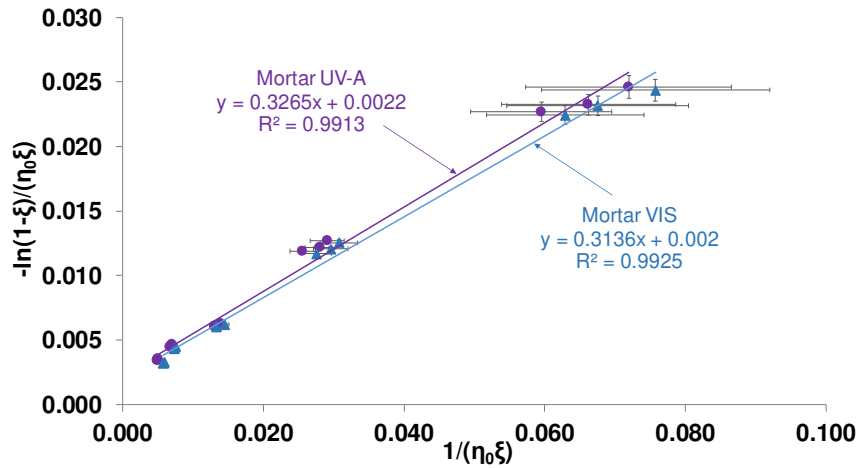


Figure 7. Variable Y versus variable X (cf. equation 11) for 100 mm long mortar samples under UV-A and visible light (VIS).

Figure 8 shows the results obtained with 250 mm long mortar and plasterboard samples for various concentrations of NO, from 100 to 400 ppb with a concentration step of 50 ppb, under visible light and UV-A light. As explained above, the variable Y was plotted as a function of the variable X . Again, a linear correlation was observed. The trend lines are indicated in Figure 8. The adsorption coefficients K obtained with the longer samples were positive for the two substrates tested under UV-A and visible light. Their values, together with those of the reaction rate constant k , are reported in Table 2. Considering the uncertainty related to the experiments, the coefficient K was assumed to be similar for both substrates and independent of the lighting conditions (errors on K were: ± 2.20 or 2.38 or 1.76 or 2.52 ppb⁻¹). However, the coefficient k seemed to be impacted by the nature of the substrate and the light (the uncertainty on the values was quite low: ± 0.07 or 0.08 ppb/min). Lower values were obtained under visible light for both substrates: $k_{UV} = 1.15 \times k_{visible}$ for mortar and plasterboard samples, and higher values were obtained for mortar: $k_{mortar} = 1.10 \times k_{plasterboard}$ for both lighting conditions. Such results were expected as the photocatalytic activity, and thus the degradation of NO, is wavelength selective and accelerated by UV light [7,28]. The semiconductor TiO₂ is activated for wavelengths below 388 nm, which explains the higher reaction rate constant k obtained under UV-A light. The degradation of NO observed under visible light could be explained by: (i) the non-zero value of the light intensity of the fluorescent tube between 380 and 400 nm (the lowest wavelength of the visible light spectrum may be considered equal to 380 nm), and/or (ii) the doping of TiO₂ nanoparticles in order to make them sensitive to the visible blue light (the formulation of the commercial product was not known). The influence of the irradiance on constants k and K was highlighted by Hunger et al. [18]. They showed that the reaction rate constant, k , was dependent on the irradiance while the adsorption coefficient, K , remained unaffected. Moreover, the synergic effect between the cementitious matrix and NO could explain the higher value of the reaction rate constant k obtained with mortar samples. Cassar notably suggested that the cement hydrates could

trap NO₂ and nitrate salt formed during the photo-oxidation of NO [29], and Horgnies et al. highlighted the reaction of NO₂ with strongly alkaline hydrates [30]. The values of K and k obtained at the reactor scale for plasterboard were used for the modelling at the experimental chamber scale.

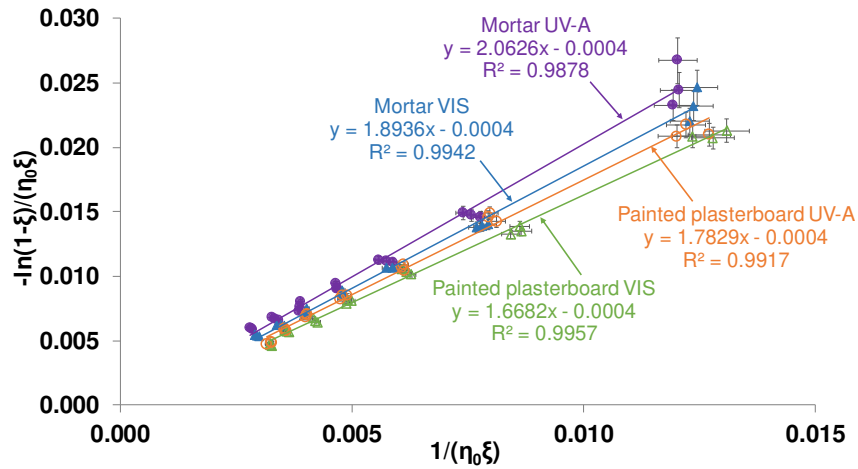


Figure 8. Variable Y versus variable X (cf. equation 11) for 250 mm long mortar and plasterboard samples under 2 lighting conditions: UV-A and visible light (VIS).

Table 2. Mean values of rate law coefficients obtained for mortar and plasterboard samples under UV-A and visible light. Adsorption coefficient K is expressed in ppb^{-1} and reaction rate constant k is expressed in ppb/min .

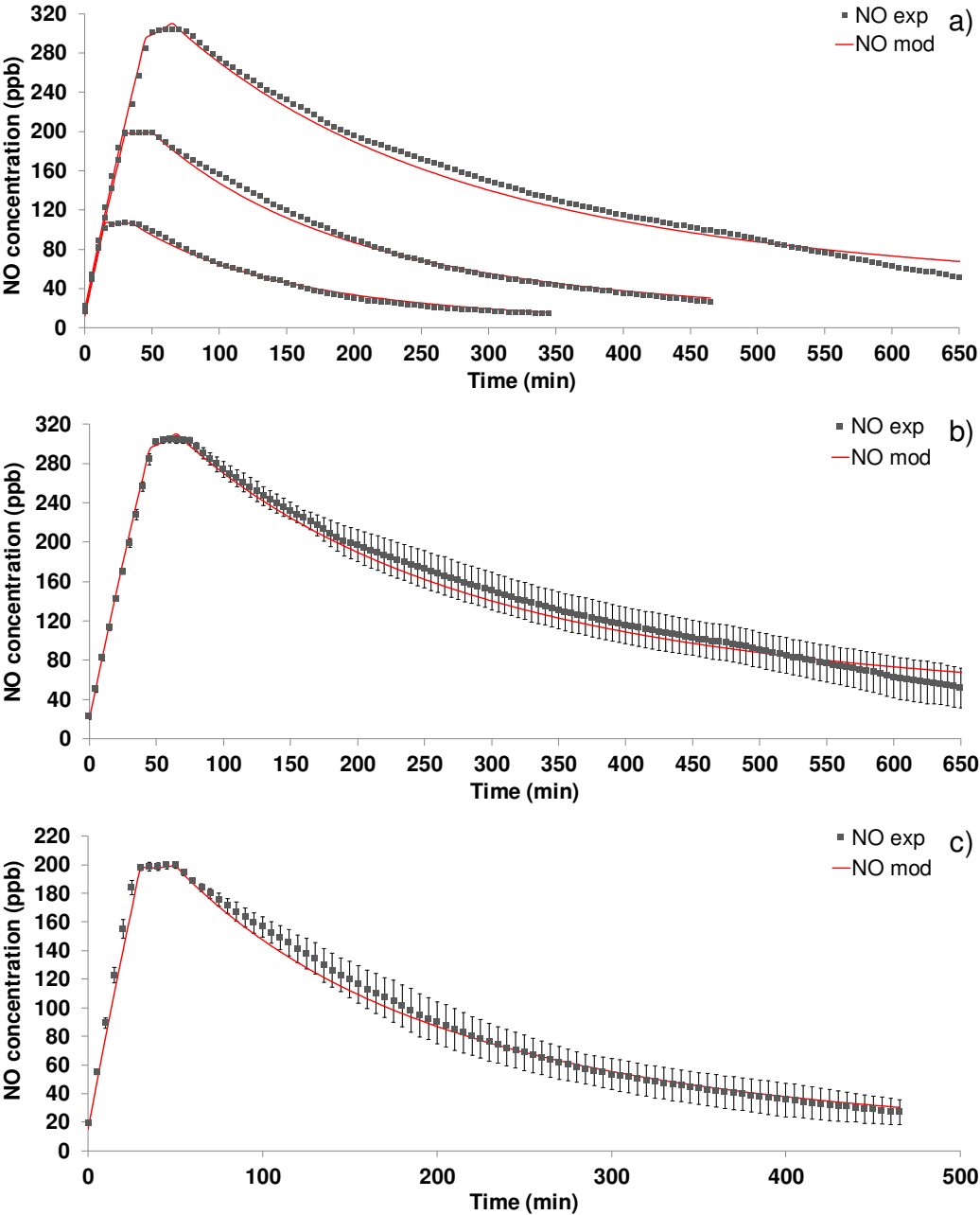
	Visible light	UV-A light
Mortar	$K = (3.91 \pm 2.20) \times 10^{-4} \text{ ppb}^{-1}$ $k = (2.42 \pm 0.08) \times 10^{+5} \text{ ppb}/\text{min}$	$K = (3.72 \pm 2.38) \times 10^{-4} \text{ ppb}^{-1}$ $k = (2.78 \pm 0.08) \times 10^{+5} \text{ ppb}/\text{min}$
Plasterboard	$K = (3.79 \pm 1.76) \times 10^{-4} \text{ ppb}^{-1}$ $k = (2.20 \pm 0.07) \times 10^{+5} \text{ ppb}/\text{min}$	$K = (3.53 \pm 2.52) \times 10^{-4} \text{ ppb}^{-1}$ $k = (2.53 \pm 0.07) \times 10^{+5} \text{ ppb}/\text{min}$

4.2. Modelling of the evolution of NO concentration in an experimental chamber

4.2.1. Without photocatalysis – step 1: Identification of the model parameters \bar{q} and α

Figure 9 shows the experimental concentrations of NO measured by the analyzer (each point is the average of three values) and the concentrations calculated with the three-flow model according to Figure 3. Experiments were carried out in the dark with three different maximum concentrations of NO (Figure 9.a): 300 ppb (Figure 9.b), 200 ppb (Figure 9.c) and 100 ppb (Figure 9.d). For the increasing phase, from 0 to 50 min, the injected flow rate (q_{inj}) was equal to 1.5 l/min for all the concentrations tested. For the constant phase, q_{inj} was reduced and depended on the value of the maximum concentration, as specified in Table 1. The injection was then stopped at 65 min for 300 ppb (Figure 9.b), 50 min for 200 ppb (Figure 9.c) and 35 min for 100 ppb (Figure 9.d), meaning that $q_{inj} = 0$. As the chamber was not airtight, the NO concentration slowly decreased. It took many hours to reach an NO concentration of several tens of ppb. The experimental data were well fitted by

the model throughout the experiment for the three concentrations tested. The parameters \bar{q} and α were identified and the following values were selected to obtain the best fit: $\bar{q} = 26 \text{ ln/min}$ and $\alpha = 0.25$. The NO outdoor concentration ($\bar{\eta}$) was not monitored and was assumed to be constant throughout a test. Its value was adjusted for each experiment in a way that best fitted the experimental points. The model response to this parameter was assessed however. Figure 10 shows the model sensitivity to different values of $\bar{\eta}$ for the experiment conducted with a maximum indoor NO concentration of 200 ppb (\bar{q} and α being unchanged). In this case, 5 ppb was the value selected for $\bar{\eta}$, as it enabled the best fit between experimental and modelled values to be obtained. To go even further, the NO outdoor concentration could be monitored with an additional analyzer and its evolution law taken into account in equation 14.



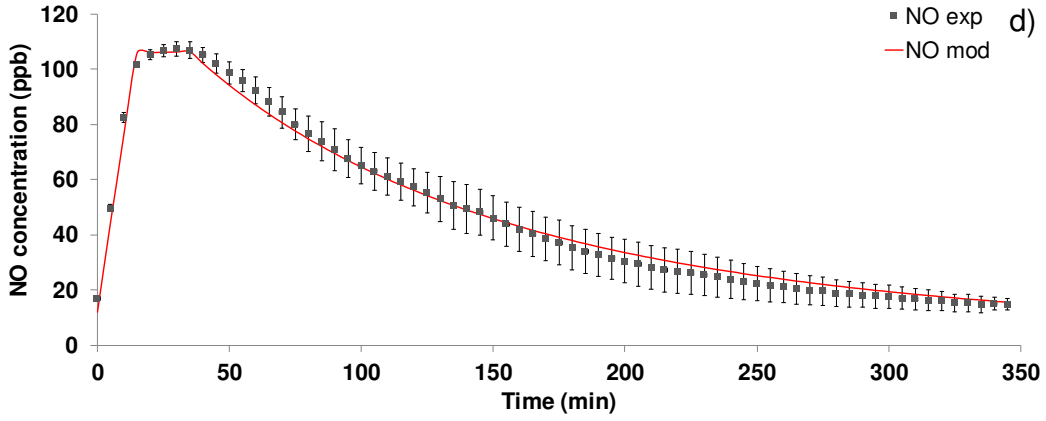


Figure 9. Comparison between the measured concentrations of NO and the values obtained with the three-flow model. Three maximum concentrations were injected: a) plots of the three concentrations, b) 300 ppb, c) 200 ppb and d) 100 ppb, at different scales.

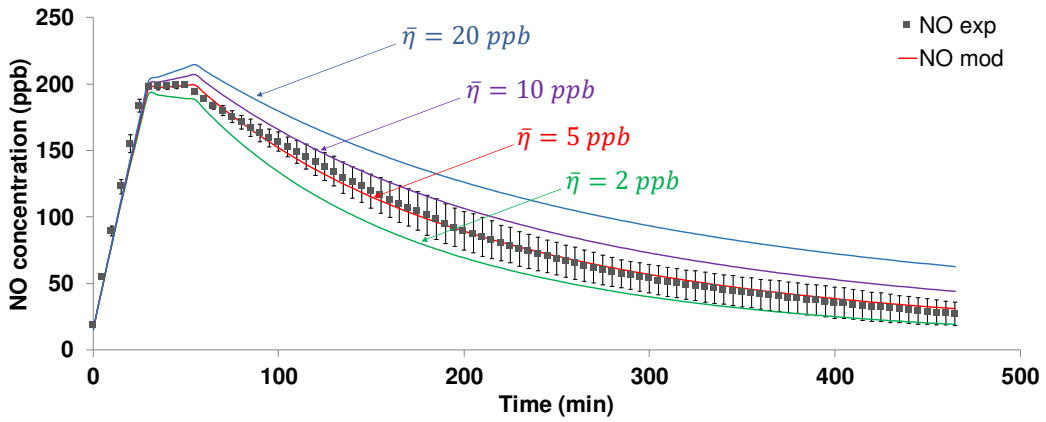


Figure 10. Model sensitivity to different values of $\bar{\eta}$ for the experiment conducted with a maximum indoor NO concentration of 200 ppb.

Moreover, the three-flow model allowed the values of the flow rates reported in Table 1 (and defined experimentally) to be calculated. During the NO injection at a low flow rate (constant level of pollution inside the chamber), the variation of the $\bar{\eta}$ concentration was taken to be 0, which meant that $\frac{d\bar{\eta}}{dt} = 0$. In such conditions, Equation 16 allows us to write:

$$\left[q_{inj} \left(\frac{\eta_{inj}}{\bar{\eta}} - 1 \right) - \bar{q} \left(\frac{\eta}{\bar{\eta}} - 1 \right)^{1+\alpha} \right] = 0 \quad (\text{eq.23})$$

Therefore, the injected flow rate during the constant phase is defined by equation 24:

$$q_{inj} = \bar{q} \frac{\left(\frac{\eta}{\bar{\eta}} - 1 \right)^{1+\alpha}}{\left(\frac{\eta_{inj}}{\bar{\eta}} - 1 \right)} \quad (\text{eq.24})$$

which gives, in the case of the experiment carried out at $\eta = 200$ ppb:

$$q_{inj} = 26 \frac{\left(\frac{200}{5} - 1 \right)^{1+0.25}}{\left(\frac{45000}{5} - 1 \right)} = 0.28 \text{ ln/min} \quad (\text{eq.25})$$

This value is consistent with the injected flow rate defined experimentally $q_{inj\ exp} = 0.30\ ln/min$ (cf. Table 1). In the case of 300 ppb, equation 24 gives $q_{inj} = 0.47\ ln/min$ ($q_{inj\ exp} = 0.45\ ln/min$). For 100 ppb, the value given by equation 24 is slightly underestimated: $q_{inj} = 0.12\ ln/min$ versus $q_{inj\ exp} = 0.20\ ln/min$.

4.2.2. With photocatalysis – step 2: Identification of the model parameter A_ϕ

Figure 11 shows the NO experimental concentrations measured by the analyzer (each point is the average of three values) and the concentrations calculated with the four-flow model according to Figure 5. Experiments were carried out only with the NO concentration of 200 ppb. The increasing concentration phase and the constant phase were obtained as described previously for step 1. However, in this case, the injection was not stopped at the end of the concentration plateau. At 50 min, the lighting was switched on to activate the photocatalysis: under UV-A (cf. Figure 11.a) and visible light (cf. Figure 11.b). The NO concentration decreased rapidly: it reached a background value of around 20 ppb after 50 min. The experimental data were again well fitted by the model. The values of \bar{q} and α obtained during step 1 were used. Step 2 allowed the parameter A_ϕ to be identified, its value being dependent on the lighting conditions; the higher the photocatalytic activity, the higher the A_ϕ value: $A_\phi = 8.561\ min^{-1}$ for UV-A light and $A_\phi = 6.640\ min^{-1}$ for visible light. The thickness e' of the diffusive zone above the plasterboard samples was therefore determined for both lighting conditions according to the following equations:

$$A_\phi = \frac{V_\phi}{V} K = \frac{S \times e'}{V} K k \quad (\text{eq.26})$$

Therefore,

$$e' = \frac{A_\phi V}{S K k} \quad (\text{eq.27})$$

where the constants K and k were determined at the reactor scale under UV-A and visible light (cf. Table 2).

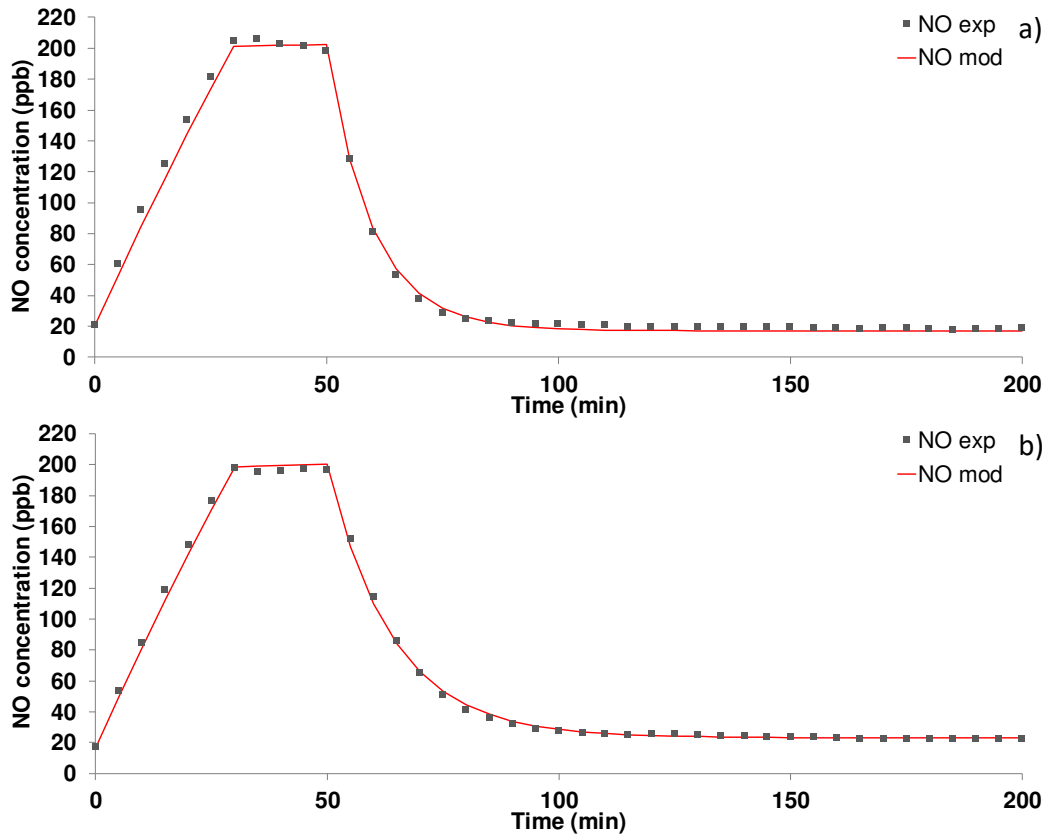


Figure 11. Comparison between the measured concentrations of NO and the values obtained with the four-flow model. A maximal concentration of 200 ppb was injected under: a) UV-A and b) visible light.

The values of the parameters of the four-flow model are summarized in Table 3. The thickness e' was dependent on the lighting conditions (98 mm for UV-A versus 81 mm for visible light): the UV-A radiation led to a higher photocatalytic thickness, and therefore to a larger spread of the reactive radicals in the air layer above the sample surfaces. The increase of e' with UV-A light was consistent with the increase of the reaction rate constant k observed at the reactor scale. Moreover, in [21], Topalov et al. compared the photocatalysis efficiency with respect to NO obtained in this experimental chamber using various lighting systems; the same fluorescent tubes as the ones used in the present study and halogen and LED bulbs in the visible spectrum. Lower NO abatement values were reported for the halogen and LED bulbs. Modelling has not yet been conducted with these two lighting systems. However, a smaller thickness e' can be expected under halogen and LED bulbs, as their lighting intensities were low for wavelengths below 388 nm.

Table 3. Parameters of the four-flow model: V and S are characteristics of the experimental chamber, K and k were determined at the reactor scale, \bar{q} and α were determined during step 1, and e' during step 2.

Parameters	Values	
	UV-A light	Visible light
V , volume of the chamber	10.3 m ³	
S , plasterboard surface area on the indoor walls	9.8 m ²	

K , adsorption coefficient	$3.53 \cdot 10^{-4} \text{ ppb}^{-1}$	$3.79 \cdot 10^{-4} \text{ ppb}^{-1}$
k , reaction rate constant	$2.53 \cdot 10^5 \text{ ppb}/\text{min}$	$2.20 \cdot 10^5 \text{ ppb}/\text{min}$
\bar{q} , flow-rate-like constant	$26 \text{ ln}/\text{min}$	
α , positive dimensionless number	0.25	
e' , diffusive zone thickness	98 mm	81 mm

4.3. Ambitions and limitations of the model

This paper constitutes a first attempt to model the photocatalytic abatement of gaseous pollutants at chamber scale and reports quite encouraging results. The model derived showed the contribution of four flows – NO injection flow rate, air leakage, air renewal and NO decreasing flow rate due to photocatalytic oxidation – on the evolution of NO indoor concentration, and allowed the thickness of the air layer involved in the photocatalysis to be estimated. Because the chamber was not airtight, leaks were observed and had to be taken into account in the model. They could not be explained by the overpressure due to the injection phase of the NO pollutant; such a phenomenon was never observed in spite of the accuracy of the barometric instruments. Instead, the leakage was explained by the difference of NO concentration between the interior and the exterior, which was expressed through an appropriate but empirical law. The percentage of decrease in the (amount of) pollution when the light was switched on was, obviously, attributed to the photocatalytic effect of the dispersion coating the plasterboard samples. This percentage did not constitute a real flow rate but nevertheless contributed to the disappearance of NO. It was taken into account through a rate law inspired by the Langmuir-Hinshelwood model. Thus, the adsorption and the abatement kinetics parameters were identified in a lab reactor. However, the following reservations should be made on the use of the L-H-like law in the four-flow model:

- The rate law has a "local" character. At lab scale, the samples had small sizes and the law was assumed to apply uniformly because the local characteristics listed here are reputed to be uniform: porosity, roughness, amount of TiO_2 at the surface of samples, lighting, temperature, humidity.
- Therefore, the generalization of the use of the rate law to a greater volume, as in the experimental chamber, necessitated the assumption that the local conditions were uniform. For instance, the lighting was implicitly averaged over the whole area of the walls.
- Another issue concerns the thickness of the air layer involved in the photocatalysis phenomenon. At reactor scale, it is generally accepted that this thickness corresponds to the distance between the surface of the sample and the borosilicate upper surface. In the case of the chamber, no equivalent assessment could be made: the model provided an answer but the order of magnitude was about 20 times larger than in the reactor (81 mm or 98 mm).

versus 5 mm). It is too early to claim that the values found in this range have physical significance.

In order to provide answers to these concerns, the model has to be refined. Further studies, like the ones listed below, need to be carried out:

- Check on the general scope of the model. New experiments could be performed with other illuminants, other substrates, other pollutants. For instance, experiments conducted with NO₂ should show a greater adsorption ability. Will this phenomenon be correctly expressed by the model?
- Measurement of the external pollution. Rather than taking a constant value for the external pollution level, the model, in its current version, already enables the real-time evolution $\bar{\eta}(t)$ to be taken into consideration.
- Introduction of a model for the illumination of the walls, provided that a correlation can be established between i) the wavelength and the intensity of the light, and ii) the coefficients k and K .

The model presented fitted the experimental data well in the specific conditions of this chamber. Improving this model according to the above suggestions could make it possible to evaluate the efficiency of various indoor air depollution techniques or devices, available commercially or as part of research works. It could even contribute to an assessment of the influence of various parameters (such as the lighting, the substrate nature, etc.) on the air depollution function.

5. Conclusion

The main aim of this study was to make a contribution to a predictive model of pollution abatement in a room. The gas targeted was nitrogen monoxide. The suggested four-flow model was built in three steps. First, the adsorption and the abatement kinetics parameters were identified in a lab reactor, using a rate law mathematically similar to the L-H model. Then, a three-flow model was developed at the chamber scale, taking the NO injection phase, the air leakage and the air renewal into account. The flow associated with the photocatalytic oxidation (occurring when the light was switched on) was introduced as a third step based on an L-H-like law. Results showed good agreement between predicted values and experimental data, meaning that the suggested models described the evolution of NO well at the experimental chamber scale. A parameter not previously considered was extracted from the four-flow model: the thickness of the diffusive zone in which the process of abatement was assumed to take place. This thickness was estimated at between 80 and 100 mm depending on the illuminant involved in the photocatalysis (visible or UV-A light). The first-intention model presented here is ambitious but suffers from several deficiencies, which could be

overcome thanks to further investigations as suggested in the discussion. Such modelling work could enable future prediction of the photocatalytic process under various environmental conditions and thus its translation towards real environments.

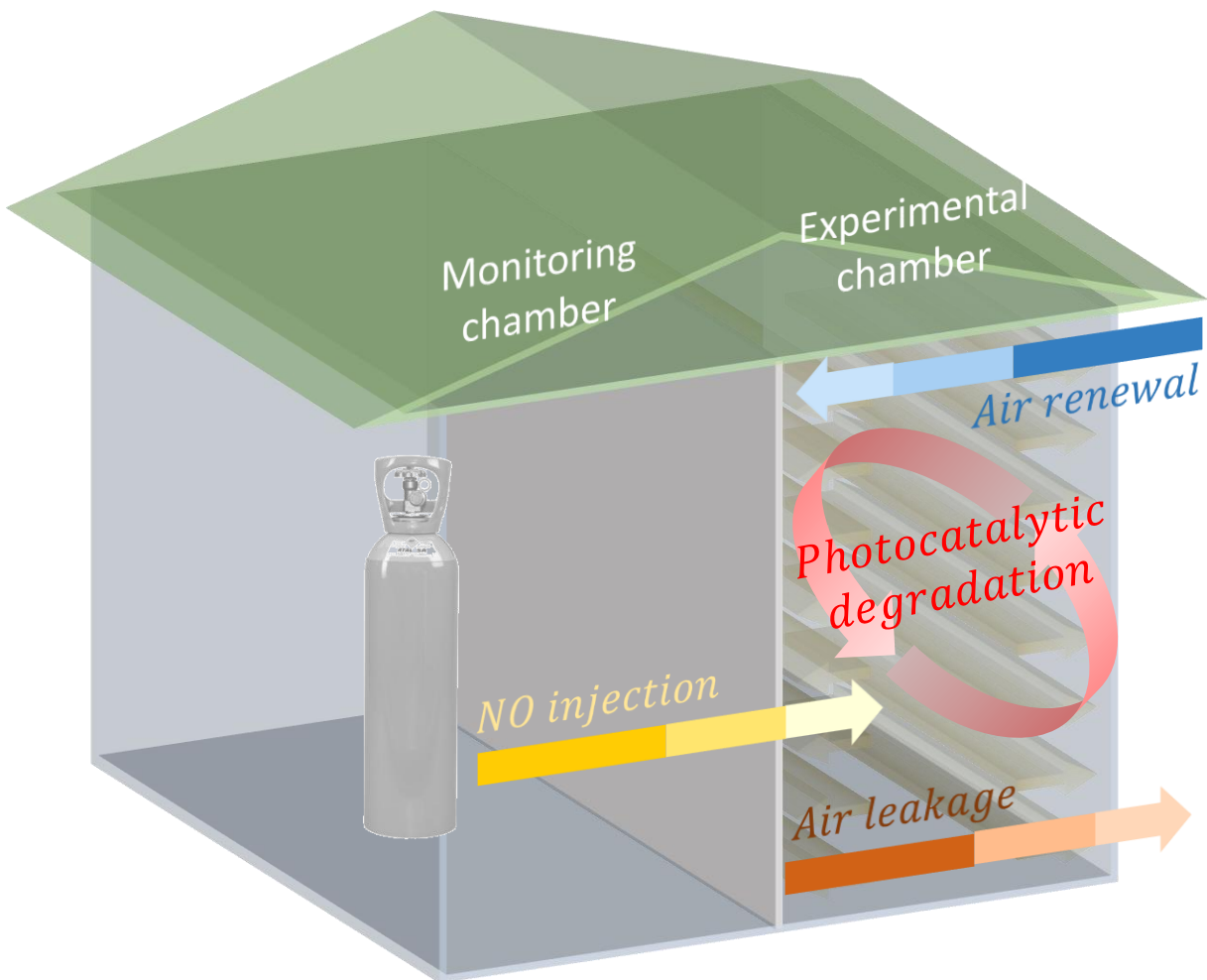
6. Acknowledgments

The authors are grateful to Mr. Jivko Topalov for his collaboration in this work, in particular his contribution to the carrying out of the experiments.

7. References

- [1] L. Sivachandiran, F. Thevenet, P. Gravejat, A. Rousseau, Investigation of NO and NO₂ adsorption mechanisms on TiO₂ at room temperature, *Appl. Catal. B Environ.* 142–143 (2013) 196–204. <https://doi.org/10.1016/j.apcatb.2013.04.073>.
- [2] Y. Boyjoo, H. Sun, J. Liu, V.K. Pareek, S. Wang, A review on photocatalysis for air treatment: From catalyst development to reactor design, *Chem. Eng. J.* 310 (2017) 537–559. <https://doi.org/10.1016/j.cej.2016.06.090>.
- [3] R. Zouzelka, J. Rathousky, Photocatalytic abatement of NO_x pollutants in the air using commercial functional coating with porous morphology, *Appl. Catal. B Environ.* 217 (2017) 466–476. <https://doi.org/10.1016/j.apcatb.2017.06.009>.
- [4] S. Ifang, M. Gallus, S. Liedtke, R. Kurtenbach, P. Wiesen, J. Kleffmann, Standardization methods for testing photo-catalytic air remediation materials: Problems and solution, *Atmos. Environ.* 91 (2014) 154–161. <https://doi.org/10.1016/j.atmosenv.2014.04.001>.
- [5] A. Mills, S. Elouali, The nitric oxide ISO photocatalytic reactor system: Measurement of NO_x removal activity and capacity, *J. Photochem. Photobiol. Chem.* 305 (2015) 29–36. <https://doi.org/10.1016/j.jphotochem.2015.03.002>.
- [6] T.N. Obee, R.T. Brown, TiO₂ photocatalysis for indoor air applications: Effects of humidity and trace contaminant levels on the oxidation rates of formaldehyde, toluene, and 1,3-butadiene, *Environ. Sci. Technol.* 29 (1995) 1223–1231. <https://doi.org/10.1021/es00005a013>.
- [7] Q.L. Yu, H.J.H. Brouwers, Indoor air purification using heterogeneous photocatalytic oxidation. Part I: Experimental study, *Appl. Catal. B Environ.* 92 (2009) 454–461. <https://doi.org/10.1016/j.apcatb.2009.09.004>.
- [8] T. Martinez, A. Bertron, E. Ringot, G. Escadeillas, Degradation of NO using photocatalytic coatings applied to different substrates, *Build. Environ.* 46 (2011) 1808–1816. <https://doi.org/10.1016/j.buildenv.2011.03.001>.
- [9] J.V.S. de Melo, G. Trichês, Evaluation of the influence of environmental conditions on the efficiency of photocatalytic coatings in the degradation of nitrogen oxides (NO_x), *Build. Environ.* 49 (2012) 117–123. <https://doi.org/10.1016/j.buildenv.2011.09.016>.
- [10] J. Hot, J. Topalov, E. Ringot, A. Bertron, Investigation on parameters affecting the effectiveness of photocatalytic functional coatings to degrade NO: TiO₂ amount on surface, illumination, and substrate roughness, *Int. J. Photoenergy.* 2017 (2017) e6241615. <https://doi.org/10.1155/2017/6241615>.
- [11] G.L. Guerrini, Photocatalytic performances in a city tunnel in Rome: NO_x monitoring results, *Constr. Build. Mater.* 27 (2012) 165–175. <https://doi.org/10.1016/j.conbuildmat.2011.07.065>.
- [12] M.M. Ballari, H.J.H. Brouwers, Full scale demonstration of air-purifying pavement, *J. Hazard. Mater.* 254–255 (2013) 406–414. <https://doi.org/10.1016/j.jhazmat.2013.02.012>.
- [13] J. Zhao, X. Yang, Photocatalytic oxidation for indoor air purification: a literature review, *Build. Environ.* 38 (2003) 645–654. [https://doi.org/10.1016/S0360-1323\(02\)00212-3](https://doi.org/10.1016/S0360-1323(02)00212-3).

- [14] H. Wang, Z. Wu, W. Zhao, B. Guan, Photocatalytic oxidation of nitrogen oxides using TiO₂ loading on woven glass fabric, *Chemosphere*. 66 (2007) 185–190. <https://doi.org/10.1016/j.chemosphere.2006.04.071>.
- [15] A. Folli, S.B. Campbell, J.A. Anderson, D.E. Macphee, Role of TiO₂ surface hydration on NO oxidation photo-activity, *J. Photochem. Photobiol. Chem.* 220 (2011) 85–93. <https://doi.org/10.1016/j.jphotochem.2011.03.017>.
- [16] Z. Khuzwayo, E.M.N. Chirwa, Modelling and simulation of photocatalytic oxidation mechanism of chlorohalogenated substituted phenols in batch systems: Langmuir–Hinshelwood approach, *J. Hazard. Mater.* 300 (2015) 459–466. <https://doi.org/10.1016/j.jhazmat.2015.07.034>.
- [17] L. Zhong, F. Haghghat, P. Blondeau, J. Kozinski, Modeling and physical interpretation of photocatalytic oxidation efficiency in indoor air applications, *Build. Environ.* 45 (2010) 2689–2697. <https://doi.org/10.1016/j.buildenv.2010.05.029>.
- [18] M. Hunger, G. Hüsken, H.J.H. Brouwers, Photocatalytic degradation of air pollutants — From modeling to large scale application, *Cem. Concr. Res.* 40 (2010) 313–320. <https://doi.org/10.1016/j.cemconres.2009.09.013>.
- [19] NF EN 196-1, Methods of Testing Cement – Part 1: Determination of Strength, (2016).
- [20] ISO 22197-1:2016, Fine ceramics (advanced ceramics, advanced technical ceramics) — Test method for air-purification performance of semiconducting photocatalytic materials — Part 1: Removal of nitric oxide, (2016).
- [21] J. Topalov, J. Hot, E. Ringot, A. Bertron, In situ NO abatement by photocatalysis—study under continuous NO injection in a 10-m³ experimental chamber, *Air Qual. Atmosphere Health*. 12 (2019) 229–240. <https://doi.org/10.1007/s11869-018-0644-7>.
- [22] J. Hot, A. Dasque, J. Topalov, V. Mazars, E. Ringot, Titanium valorization: From chemical milling baths to air depollution applications, *J. Clean. Prod.* 249 (2020) 119344. <https://doi.org/10.1016/j.jclepro.2019.119344>.
- [23] J. Hot, T. Martinez, B. Wayser, E. Ringot, A. Bertron, Photocatalytic degradation of NO/NO₂ gas injected into a 10-m³ experimental chamber, *Environ. Sci. Pollut. Res.* 24 (2017) 12562–12570. <https://doi.org/10.1007/s11356-016-7701-2>.
- [24] J. Peral, D.F. Ollis, Heterogeneous photocatalytic oxidation of gas-phase organics for air purification: Acetone, 1-butanol, butyraldehyde, formaldehyde, and m-xylene oxidation, *J. Catal.* 136 (1992) 554–565. [https://doi.org/10.1016/0021-9517\(92\)90085-V](https://doi.org/10.1016/0021-9517(92)90085-V).
- [25] M. Sleiman, P. Conchon, C. Ferronato, J.-M. Chovelon, Photocatalytic oxidation of toluene at indoor air levels (ppbv): Towards a better assessment of conversion, reaction intermediates and mineralization, *Appl. Catal. B Environ.* 86 (2009) 159–165. <https://doi.org/10.1016/j.apcatb.2008.08.003>.
- [26] S. Devahasdin, C. Fan, K. Li, D.H. Chen, TiO₂ photocatalytic oxidation of nitric oxide: transient behavior and reaction kinetics, *J. Photochem. Photobiol. Chem.* 156 (2003) 161–170. [https://doi.org/10.1016/S1010-6030\(03\)00005-4](https://doi.org/10.1016/S1010-6030(03)00005-4).
- [27] M.M. Ballari, M. Hunger, G. Hüsken, H.J.H. Brouwers, Modelling and experimental study of the NO_x photocatalytic degradation employing concrete pavement with titanium dioxide, *Catal. Today*. 151 (2010) 71–76. <https://doi.org/10.1016/j.cattod.2010.03.042>.
- [28] G. Hüsken, M. Hunger, H.J.H. Brouwers, Experimental study of photocatalytic concrete products for air purification, *Build. Environ.* 44 (2009) 2463–2474. <https://doi.org/10.1016/j.buildenv.2009.04.010>.
- [29] L. Cassar, Photocatalysis of Cementitious Materials: Clean Buildings and Clean Air, *MRS Bull.* 29 (2004) 328–331. <https://doi.org/10.1557/mrs2004.99>.
- [30] M. Horgnies, I. Dubois-Brugger, E.M. Gartner, NO_x de-pollution by hardened concrete and the influence of activated charcoal additions, *Cem. Concr. Res.* 42 (2012) 1348–1355. <https://doi.org/10.1016/j.cemconres.2012.06.007>.



Experimental data

+

Finite difference approach and Least-squares method

=

Four-flow model to predict NO photocatalytic abatement and air layer thickness affected by photocatalysis

